Ghost Imaging Using Optical Correlations

Paul-Antoine Moreau*, Ermes Toninelli*, Thomas Gregory, Miles J. Padgett†

SUPA, School of Physics and Astronomy, University of Glasgow, Glasgow, G12 8QQ, UK

26th May 2017

1. Introduction

Conventional camera systems use light that is transmitted by, or back-scattered from, the object to form an image on a film or focal-plane detector array. By contrast, ghost imaging systems use spatial correlations between separated optical fields to obtain images without the need to record the image itself. In a ghost imaging system, the principal detector is a single-element (or single-pixel) device that measures the interaction between a single photon position (or optical pattern) and the unknown object. The other, spatially correlated photon, does not interact with the object but it own position is measured using an imaging system. This article seeks to explain both quantum ghost imaging techniques – i.e. ghost imaging techniques where correlations are quantum in their origin, and classical ghost imaging techniques – i.e. ghost imaging techniques that harness classical correlations. The article will also highlight where these techniques might have practical applications.

2. Ghost Imaging using parametric downconversion

The term "ghost imaging" was introduced in the description of the work reported by Shih and co-workers [1,2] in the 1990's following theoretical works by Klyshko [3,4]. They used the quantum correlation between the signal and idler beams produced as a result of parametric downconversion to create an alternative kind of imaging system. Figure 1 displays the ghost image captured by Shih and co-workers [2].

† Corresponding Author e-mail: Miles.Padgett@glasgow.ac.uk
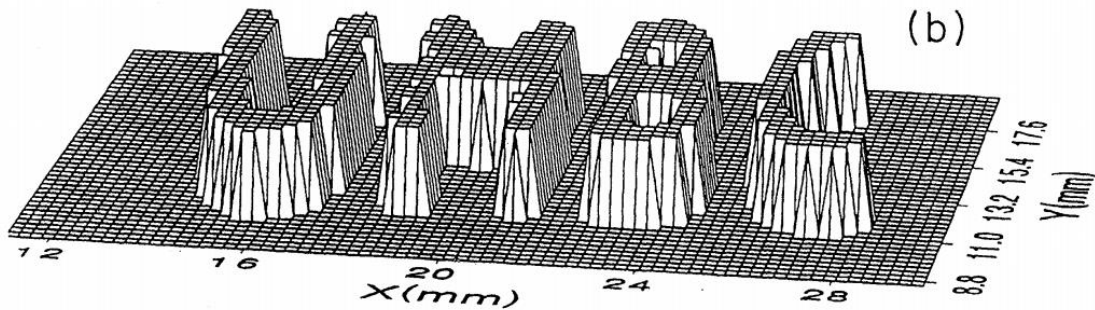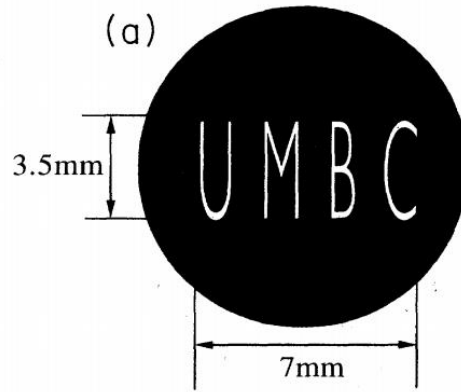
* These authors contributed equally

Figure 1 First ghost image reconstruction by Shih and co-workers. The UMBC logo (a) is reconstructed using the ghost imaging technique by exploiting correlated photons detected using single photon avalanche photodiodes that are translated so as to reconstruct a spatially resolved image (b). Figure reproduced from ref. [2].

The process of parametric downconversion occurs when a light beam is incident upon a nonlinear optical crystal [5] . The nonlinearity of the crystal refers to the functional relationship between the applied electric field (associated with the incident light) and the resulting polarisation of the material, the sinusoidal form of the incident optical field resulting in a non-sinusoidal polarisation. This non-sinusoidal response corresponds to a harmonic distortion of the electric field and hence an incident light beam with frequency of ω results in some light emitted with frequency 2ω, a phenomenon called second harmonic generation which is widely used in commercial systems to convert an infrared laser into one with a visible emission. More subtly, a similar process can take an incident pump beam of frequency ω_p and downconvert it into signal and idler beams of frequencies ω_s and ω_i, where $\omega_p = \omega_s + \omega_i$. In terms of photons it is useful to think of a single pump photon being downconverted into two photons, termed signal and idler [6,7]. This

downconversion process is subject to the standard energy and momentum conservation laws.

In addition to constraining the frequencies of the downconverted light, the conservation of energy means that the downconverted signal and idler photons are generated at the same position within the crystal. Simultaneously, the conservation of transverse momentum imposes a momentum anticorrelation between signal and idler photons (i.e. $\boldsymbol{k}_p^\perp = \boldsymbol{k}_s^\perp + \boldsymbol{k}_i^\perp$, where $\boldsymbol{k}_p^\perp$, $\boldsymbol{k}_s^\perp$ and $\boldsymbol{k}_i^\perp$ are the transvers wave-vectors of the pump, signal and idler beams respectively). It is these position or momentum correlations that lie at the heart of the quantum ghost imaging technique. A quantum ghost imaging system uses these signal and idler photons to illuminate the imaging detector and the object respectively, see Figure 2.

By configuring the crystal to give collinear, phase-matching the signal and idler beams resemble spatially incoherent extended sources similar to what might be
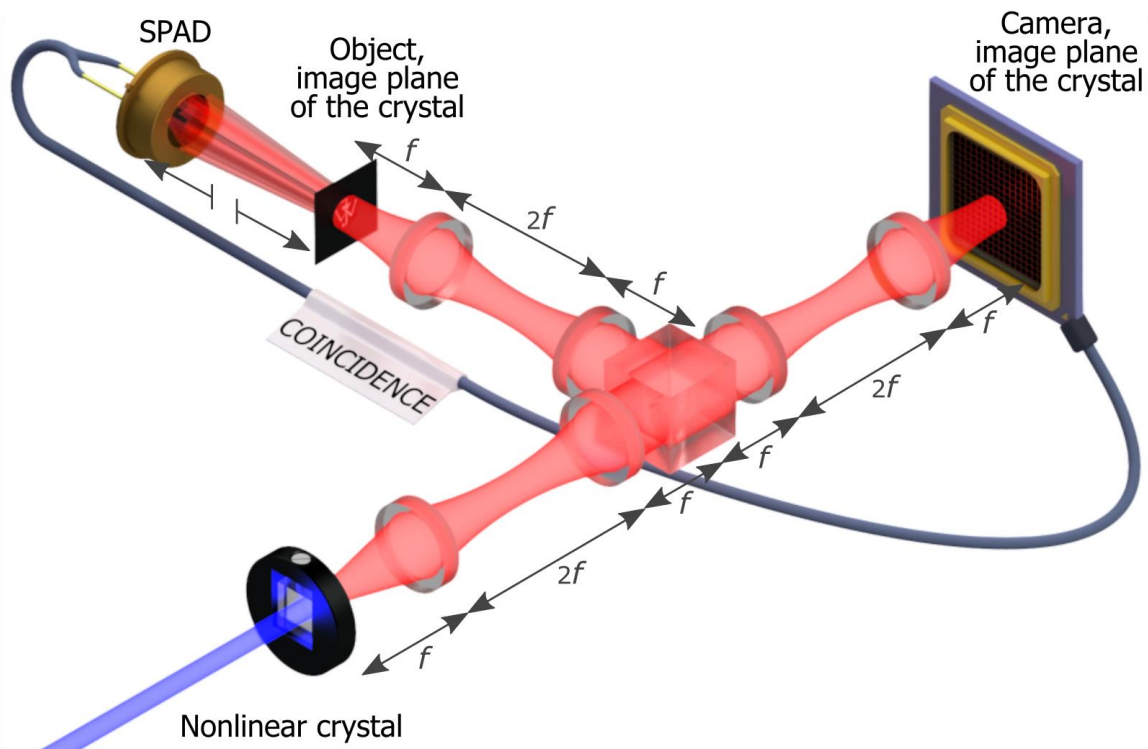
Figure 2: Quantum Ghost imaging setup, 'Image plane' configuration. Correlated photons are generated in a nonlinear crystal pumped by an UV laser. The photons are separated by a beam splitter. The center of the crystal is imaged on both the object and the camera. In order to retrieve the ghost image, the coincidences between the Single-photon avalanche diode (SPAD) and the camera are recorded. As indicated by the broken arrows the position of the SPAD relatively to the object is unimportant, the only requierment being that it collects the full ligth beam to act as a 'bucket detector'.

used in a conventional imaging system. However, the signal and idler still need to be separated from each other into separate optical paths. In the case of type-II phase-matching, the signal and idler have orthogonal polarisations and this separation can be achieved using a polarising beam splitter to create the two paths with high efficiency. However, in the case of type-I phase-matching, the signal and idler polarisations are identical and, if also near degeneracy, the only option to separate them is to rely on a simple beam splitter to separate the signal and idler photons with an inherent separation efficiency of 50%.

3. Ghost imaging using position or momentum correlations

In one possible configuration, the plane of the crystal is imaged to the plane containing the object after which a large-area, single-pixel detector detects any transmitted idler photons. This single-pixel detector is often called the "bucket detector" to acknowledge both its large area and non-imaging nature. In a separate optical path, the plane of the crystal is also imaged to a plane containing an imaging detector that measures the position of the signal photons. In the early systems, this detector relied upon raster scanning over the field of view, limiting the collection efficiency of the system to be the reciprocal of the number of scan positions that made up the image [1,2,8]. Clearly, neither the single-pixel, nor imaging detectors by themselves acquire sufficient data to deduce an image of the object. Taking the data from the imaging detector alone we see that all signal photons emitted from the source have an equal chance of being detected and hence the image formed is simply an image of the source (in this case with a spatial extent corresponding to the diameter of the pump beam). Taking the data from the bucket detector we see that only those photons that were transmitted by the object are recorded, but since their spatial position is unknown, again no image can be reconstructed. However, if the measurements of the two detectors are correlated together, an image can be reconstructed. One embodiment of this approach is when the bucket detector is used to gate, or trigger, the recording of the position of the correlated photon. This position recording can be accomplished using a triggered camera (as described later), and the image is formed by summing over many single-photon events, as seen

in Figure 3. Alternatively, the outputs of the two detectors can be combined such that only the coincident events are recorded as image information, with the image being the sum of these many correlated events.

Note that the original demonstration of ghost imaging [2] was based on a slightly different setup than that presented in Fig. 2: originally a unique lens in one of the arms was used to demonstrate the existence of a peculiar two-photon thin-lens equation, resulting in the acquisition of a ghost image.
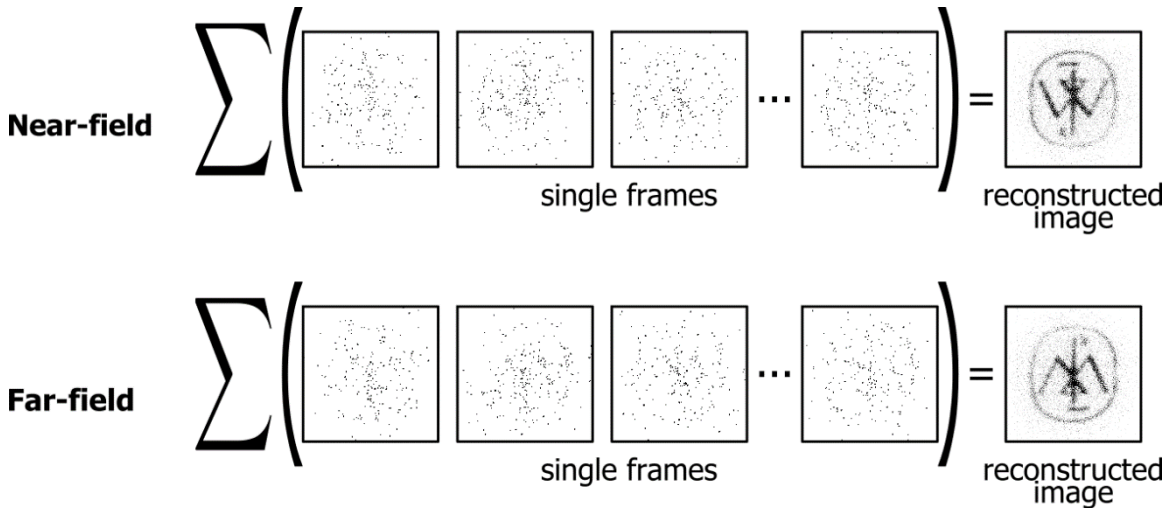

Figure 3: Reconstruction of a ghost image by summing single frame with a few photons obtained when the camera is gated conditioned on the detection of a photon by the SPAD in both image plane and far field configurations.

In essence the confirmation of transmission from the bucket detector is used to identify a sub-set of photons recorded by the imaging detector, and this sub-set of photons defines the image (akin to post selection). Essential in this imaging process is that the transverse position of the signal photons on the imaging detector are highly correlated with the positions of the idler photons in the plane of the object. This condition is ensured since, as described above, the plane of the crystal is imaged both to the imaging detector and the object (note that since the bucket detector is non-imaging it can be positioned in any plane subsequent to the object, providing that its aperture is sufficiently large to collect the transmitted photons). However, there is an alternative to this image-plane configuration. Rather than imaging the plane of the crystal to the object and imaging detector, the object and

the imaging detector can both be positioned in the far-field of the crystal, see Figure 4.
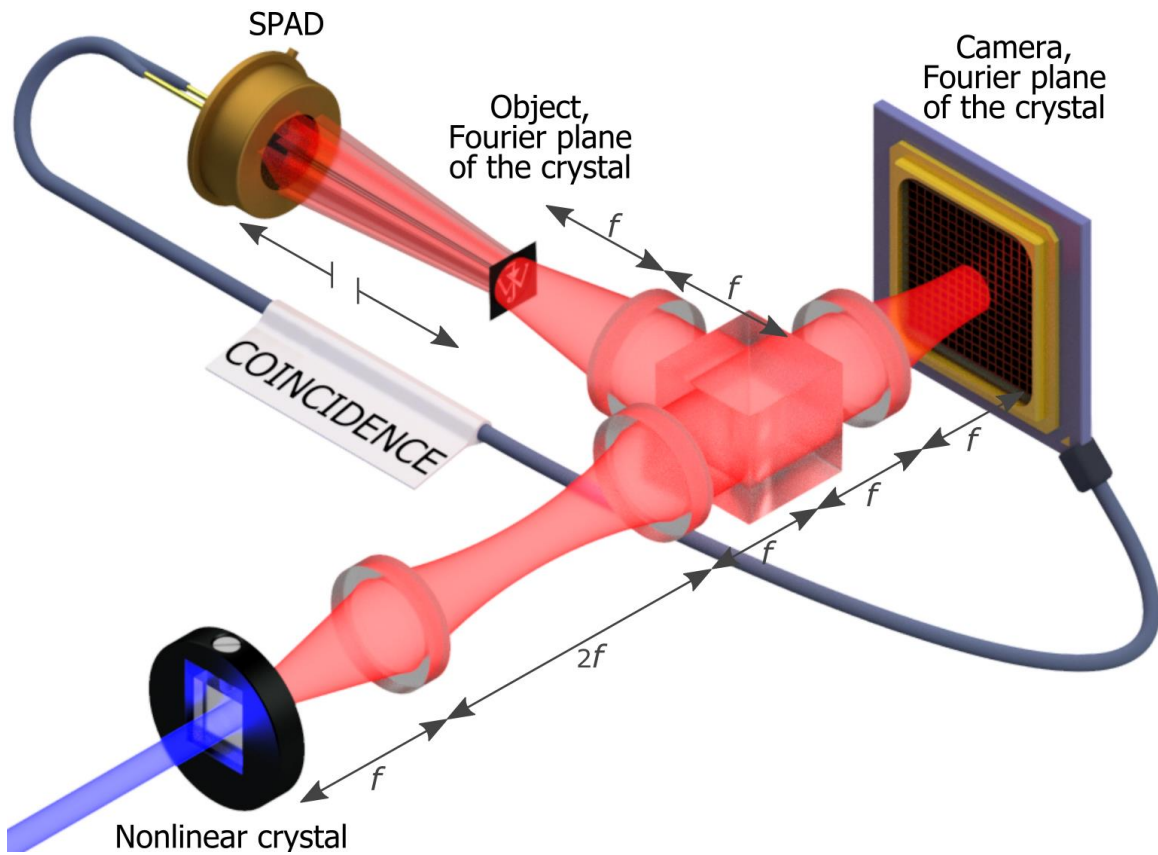
Figure 4: Quantum Ghost imaging setup, 'far-field' configuration. The spatial spectrum of the light generated inside the crystal (Fourier plane) is imaged onto both the object and the camera. The position of the SPAD relatively to the object is unimportant.

In the far-field, it is the momentum anticorrelation that means the signal and idler photons are now anticorrelated in their transverse position. Interestingly, the switch from correlation to anticorrelation means that the reconstructed image is now inverted with respect to the object see Figure 3.

It is tempting to believe that since parametric downconversion is widely used as a source of quantum-entangled photons, then ghost imaging must itself be a uniquely quantum phenomenon. However, this is not the case [9] and it has been a long-standing debate whether or not ghost imaging could be demonstrated by harnessing only classical correlations – i.e. using a scheme in which one can explain ghost imaging of an object by using only a classical light theory and a semi-classical

theory for photodetection as opposed to having to use a full quantum light theory and quantum photodetection theory. A number of studies have been conducted to determine whether or not one could reproduce quantum ghost imaging features classically [10–18].

That ghost imaging works is solely a result of the correlation between the transverse spatial position of the photons [17,18], albeit this correlation can be a result of the entanglement between the signal and idler photons. As an alternative to the entanglement inherent in parametric downconversion one could instead conceive of photon-pair sources based on purely classical, albeit complicated, scanning systems that emit position-correlated photons. Similarly a redesign of the classical system could also emit position anticorrelated photon pairs. In this respect the downconversion source is different in that the photon pairs from the same source are found to be correlated in either position or momentum depending only on the basis of the measurements made [19,20]. Therefore the capability of the downconversion source to give either upright or inverted images respectively in the image or Fourier plane of the crystal is a consequence of an EPR-type entanglement between the photons [21]. In this last respect a ghost imaging system based on downconversion does rely upon quantum correlations [22]. It is also to note that using quantum correlations for imaging presents also an advantage in term of noise reduction as discussed below [23].

4. Improving the detection efficiency of a ghost imaging system

As discussed above, using a scanning detector as the imaging detector is inherently inefficient, having a maximum detection efficiency equal to the reciprocal of the number of independent pixels in the image. Obviously, a preferred solution would be to use a detector array covering the entire field of view such that no photons are missed. Until recently, camera systems did not have the performance required to identify a single photon against the background noise. However, modern time-gated intensified CCD (ICCD) arrays are capable of detecting single photons against a virtually noise-free background, providing that their gate-time is kept short to the

order of a few nanoseconds. In this respect, ICCDs are the ideal cameras for inclusion into a ghost imaging system where the single-pixel detector heralds precisely the arrival time of the correlated photon. Gating the intensified camera in this way allows an image to be accumulated photon-by-photon, potentially acquiring thousands of individual photons [22,24]. Since most intensified cameras allow the intensifier to be triggered many thousands of times a second before the data is read out from the array, the spatially isolated photon detection events dominate over the much smaller number of rogue noise events.

5. Reconstructing images from photon sparse data

Even images containing several thousand photons appear extremely noisy. This noise arises since there are only a handful of photons per pixel and the reconstructed image of the object is subject to large pixel-to-pixel fluctuations due to the inherent shot noise resulting from the finite number of discrete photon detections. In the limit of high photon number, an expectation of n photons per pixel has an uncertainty of $\pm\sqrt{n}$ in accordance with Gaussian statistics. For lower photon number the distribution of photon counts is described by a Poissonian (no negative values). However, real images are not random collections of pixel values, typically there are strong correlations between neighbouring pixels in the image meaning that the spatial Fourier-transform of the image is sparse (i.e. has many zeros and/or very small values). This sparsity lies at the heart of image compression algorithms used to store images within a minimum amount of memory such as JPEG, and it is also used widely in image processing as the basis of de-noising algorithms where spatial frequencies of low magnitude (and hence likely to be noise) are removed from an image. The de-noising approach is further aided by, in this case, having exact knowledge of the noise model, allowing the sparsity condition to be precisely applied to reconstruct an estimate of the image with highest sparsity (in the spatial frequency domain) that is still consistent with the measured data given the known noise type. Remarkably it is possible to reconstruct a reasonable quality grey-scale image with fewer than one measured photon per image pixel, which corresponds to an intensity orders of magnitude less than a

traditional imaging system [25–27]. Note that other computational imagers employing similar hypotheses and conventional optical setups have been used for photon-efficient formation of high-quality reflectivity and depth images [28,29]. Figure 5 shows the reconstruction of photon-sparse ghost images using quantum correlations between photon pairs. The configuration used to record these ghost images is similar to the one presented in Figure 4 and the detection scheme as reported in [27], uses an Intensified CCD camera triggered by a single avalanche photodiode (SPAD) acting as the bucket detector. The photons in the camera arm travel through an image preserving delay line such that the camera gating time, as triggered by the SPAD is synchronised with the arrival of the camera arm photon. The individual frames containing the detected photons are then summed to obtain the presented images. The images are subsequently denoised by using a search algorithm aiming to maximize the sparsity of the contributing spatial frequencies in the images while maintaining the likelihood of the resulting image within the bounds set by the Poissonian statistics of the original data.
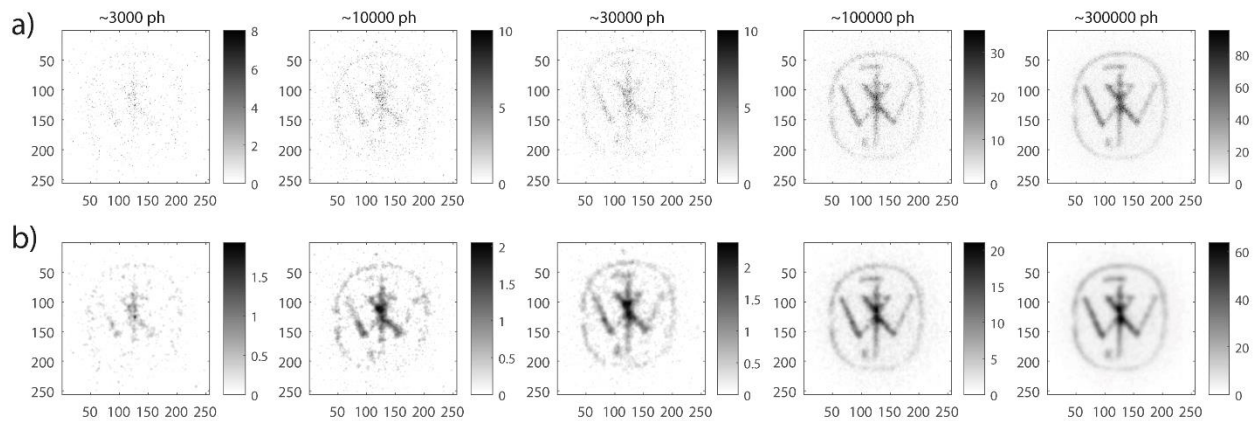
Figure 5: Ghost images obtained using quantum correlations for different numbers of photons per image, as indicated by the number above each column. The two lines of images correspond to a) summed binary images of photon detections b) images obtained through image regularisation of the above ghost images. The colorbars correspond to the number of photons per pixel. The images are composed of 256x256 pixels.

6. Ghost imaging and wavelength conversion

Beyond the recording of images with very few photons, ghost imaging based upon parametric downconversion can do other things too. Perhaps implicit in the discussion so far is that the downconversion process is degenerate, namely that the

signal and idler photons have the same wavelength, i.e. $\omega_s = \omega_i = \omega_p/2$, but this need not be the case. While still satisfying the conservation of energy, the ratio between the signal and idler wavelengths is set by the conservation of linear momentum within the nonlinear crystal. Depending upon the crystal type, changing the angle or the temperature of the crystal changes the refractive indices of the crystal, this thereby changes the optical momentum of the signal and idler photons and hence changes their wavelength ratio. Even when far away from degeneracy, such that the idler and signal have wavelengths in the infrared and visible respectively, the photons are still strongly correlated in their position and anti-correlated in their transverse momentum [30]. This means that the ghost imaging approach still works, but that the object can be probed using a different wavelength than measured by the camera. For example, the object can be probed in the short-wave infrared and the transmitted photons detected using a single-element detector, whereas the camera detector is exposed to higher energy, visible photons at a wavelength for which the camera has single-photon sensitivity [31].

Although this form of wavelength conversion still requires a detector operating at the longer wavelength, it need not be a spatially resolved one. However, there is an alternative configuration in which even the single-pixel detector is not required [32]. When using two downconversion crystals they can be arranged such that both are pumped from the same source, and the idler photons from one source pass through the other. Under these circumstances, the actual source of the idler photons is indistinguishable, as it could be either of the two crystals. This indistinguishability between the sources of the idler photons implies an interference between the two possible sources of the signal photons, and the subsequent routing of the signal photons at a beam splitter. Placing an object in the idler path between the two downconverted photon sources imposes a spatial variation on the distinguishability of the idler source and hence a spatial variation on the routing of the signal photons at the beam splitter. Hence the spatial variation of the object as illuminated by the idler is mapped to the signal even though the idler itself is never detected. In this system, the only detector that is required is an imaging array

sensitive to the signal wavelength. Despite this seemingly quantum process, as for quantum ghost imaging itself , it has been suggested that this scheme also has a classical counterpart with which it shares a number of features [33]

Ghost imaging configurations based upon differing signal and idler wavelengths create other opportunities too. Beyond imaging systems, wavelength conversion can be applied to other sensor systems, the most obvious being spectroscopy. With similar advantages, as for the imaging system, the sample can be illuminated at one wavelength and the correlated spectral information recorded at a more convenient wavelength for which the multichannel spectrometer is more sensitive [34].

7.   A classical simulator for ghost imaging

The behaviour of a ghost imaging system based upon parametric downconversion can be analysed through standard quantum techniques, however, as recognised shortly after its conception, the results of such a system could also be predicted using classical optics. Referred to as a Klyshko picture or back-projection, the single-pixel detector is notionally replaced with an optical source that is directed through the object and back to the downconversion crystal [8]. The crystal then acts as a mirror and reflects the light to the camera, which in turn records an image. This image is exactly what would have been obtained from the ghost imaging system (at least in the case of a degenerate system). However, there are clearly differences too. For example, in the downconversion system the two detected events are simultaneous in time, with the potential to be separated both in space and time. Indeed it is the observation of simultaneous, space-separated correlations that lie at the heart of quantum mechanics and is the essence of its "spookiness". By contrast in the back-projection system, the emission process and subsequent detection are sequential. However, within the Klyshko picture, the back-projection system illustrates beautifully the upright and inverted nature of the images, corresponding to the object/camera being in the image plane or far-field of the crystal (mirror). In experimental practise the change between the downconversion and the back-propagation systems is easy to implement. It is usual for the single-pixel detector to

be fibre coupled, so that a change from detector to source simply involves the reconnection of one fibre, launching light directed to the crystal. The facet of the downconversion crystal then acts as a mirror redirecting the light to the camera. As such, the back-projection system, in addition to being a classical simulator of a quantum system, can also be used as a handy alignment tool [35].

8. Ghost diffraction

In addition to ghost imaging it is possible to configure these type of systems for ghost diffraction [1,36]. In the early demonstrations the ghost diffracting object was placed in an arbitrary position, but it is also possible to obtain the exact Fourier diffraction pattern [37] by placing the object and the camera in the image and far-field plane of the downconversion crystal respectively (or vice versa), see Figure 6. Again, the back-propagation concept discussed above gives insight to the required configuration. When trying to observe a classical diffraction pattern, for example from a double slit, one needs to ensure that the illuminating light is spatially coherent. This spatial coherence needs to be mimicked in the downconversion system too, hence the bucket detector needs to be modified such that it detects only a single spatial-mode. In practise this modification is often quite simple. Under normal use, the bucket detector comprises a single-photon avalanche detector, coupled to the detection plane using an optical fibre. If this fibre is a multi-mode fibre then the detector acts as a large area, multi-mode bucket detector. Alternatively, using a single-mode fibre converts the bucket detector to a single-mode detector, hence enabling ghost diffraction [37]. Clearly, incorporating this additional degree of modal selection into the bucket detector reduces the data rate of the system, meaning the diffraction pattern takes longer to acquire than the equivalent image would. In this respect, it is no different from a classical system where spatially filtering an incoherent light source results in a reduction in intensity in proportion to the modal selectivity of the filter. Note finally that hybrid schemes using both diffraction and imaging allow heralded phase-contrast imaging to be performed through introducing a phase filter in a Fourier plane of the crystal [38].
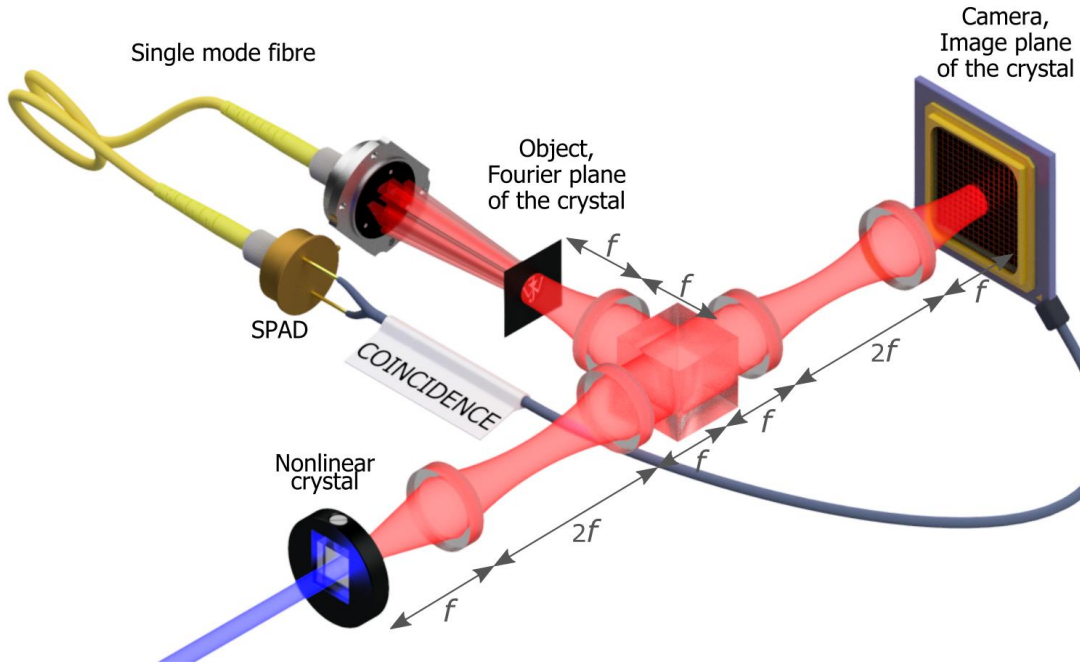
Figure 6: Quantum Ghost diffraction scheme. The object is placed in the Fourier plane of the crystal and the camera is placed in the image plane of the crystal, or conversely the object and camera are placed in the image plane and the Fourier plane respectively. The ghost diffraction images are obtained in the same manner as in the quantum ghost imaging schemes.

9. Resolution limits of ghost imaging

Quantum ghost imaging relies upon the spatial correlation or momentum anticorrelation between the signal and idler photons as produced by the parametric downconversion process. If the object is positioned in an image plane of the crystal then the field of view σ_v of any resulting imaging system depends upon the width of the pump beam, $\sigma_v = w_p$. Alternatively, if the object is placed in a far-field of the crystal, the field of view depends upon the divergence of the downconverted light and the focal length, f, of the lens creating the far-field plane. This divergence of light from the crystal is a function only of the wavelength of the light and the length of the nonlinear crystal. If one assumes when the signal and idler photons are exactly collinear with the pump photons that the phase matching is perfect ($\boldsymbol{k}_p = \boldsymbol{k}_s + \boldsymbol{k}_i$), then an angular deviation, α, for the signal and idler from co-linearity brings a phase mismatch of,

$$\Delta k_z = k_p - 2\cos(\alpha)k_s \approx (1 - \cos(\alpha))k_p \approx (\alpha^2/2)k_p.$$

For efficient generation of signal and idler over the length, L, of the nonlinear crystal this phase mismatch should not exceed $\approx \pi$ meaning that the divergence of the downconverted light is approximately given by

$\alpha^2 \lesssim 2\pi/(k_p L)$. Giving a far-field field of view $\sigma_v \approx f\sqrt{2\pi/(k_p L)}$.

More subtle than the limitations on the field of view are the factors covering the resolution of the ghost imaging system. Leaving aside the normal resolution limitations arising from the diffraction limit associated with finite aperture lenses, the resolution cannot exceed the strength of the spatial resolution between the signal and idler photons [39]. In the image plane of the crystal this correlation is closely related to the divergence of the downconverted light (since spatial localisation in the transverse plane implies divergence) and has a standard deviation given by $\sigma_c \approx 2\sqrt{2L/(\pi k_p)}$.

Alternatively if the imaging system is configured with the object and camera in the far-field then the position correlations between signal and idler photons stem from the momentum correlations in the source which in turn arise from the transverse momentum uncertainty in the pump beam. This momentum consideration gives a spatial correlation between the signal and idler photons in the far field given by

$\sigma_c \approx 4f/(k_p w_p)$.

Notwithstanding the strength of either of these correlations, the resolution of the ghost imaging system cannot exceed the resolution by which the plane of the nonlinear crystal (or, for momentum correlations, its far field) is imaged to either the object or the camera. In other words, if the resolution of the imaging system is to be limited only by the intrinsic correlation strength of the source [39], then the relay optics between source and camera/detector need to be of sufficient aperture to collect and image all of the downconverted light [18].

A further consideration as to the resolution of such a system is to recognise that a ghost imaging system can be set up in a number of seemingly equivalent

configurations. Taking the case when object and imaging detector are positioned in image planes of the nonlinear crystal, one could use additional optics to introduce additional intermediate image planes within both the camera and the single-pixel detector beam paths. In principle an image could be recorded with the object positioned in any one of these planes. If the object is placed in any image plane in the beam path of the single-pixel detector, then the system is a ghost imaging system, and the resolution limit is set as discussed above. If however, the object is positioned in the beam path of the camera detector, then an image is still recorded but the purpose of the single-pixel detector is now simply to gate (i.e. herald) the camera, such that stray light and other noise sources may be supressed [27]. An interesting question one could ask is: "Do the two types of configuration give rise to an image of the same resolution?". As discussed above, in the case of a ghost imaging system, the resolution is ultimately limited by the strength of the spatial correlations between the signal and idler photons. Clearly, the observed strength cannot exceed the resolving power of the optics, it can however be lower, according to the limits imposed by the employed nonlinear crystal. In contrast to this, for a heralded imaging system, the only factor governing the resolution is the resolving power of the optics in the camera beam path, i.e. the optics placed between the object and the camera itself.

With regards to pseudothermal ghost imaging, systems utilising classical correlations from a pseudothermal light source, the resolution is limited by the speckle size in the object plane. The transverse coherence radius of the speckle pattern may be described by the Van Cittert-Zernike theorem [40,41] thereby allowing the spatial resolution of the pseudothermal ghost imaging system to be determined [42]. This coherence radius is found to be to be of the order $dx = \lambda L/a_0$, in which the radius dx is determined by the wavelength λ of the pump used to illuminate the diffuser, the radius of the beam in the diffuser plane a_0, and L the distance of the object plane from that of the diffuser plane, or source of the speckle pattern [42,43].

For other theoretical consideration on the resolution limits in Ghost imaging the reader can refer to [44].

10. Other imaging systems based on parametric downconversion sources

In a ghost imaging system, the accumulation of data occurs photon by photon with each signal photon being correlated to an idler photon detection. The ability to image the position of a single signal photon relies upon the heralding of its arrival through the detection of the correlated idler photon. This timing precision allows a system where the camera is active only at the instant of photon arrival and thereby largely eliminates dark-counts from the image. Alternatively, if a camera system is placed in both signal and idler paths then no such heralding signal is possible and the cameras can no longer unambiguously detect a single photon against the background noise. However, if the camera exposure is set to such that many photon pairs are present in each read-out frame then correlations arising from the photon pair nature of the light can still be observed. This can be detected either as an overall correlation in the random intensity fluctuations of the signal and idler fields [45] or at the level of a small number of photons pairs [46,47]. In this latter case by setting the flux such that the number of photon pairs recorded is comparable to the number of dark events per frame it is possible to observe the overall correlation (in the image plane) or anti-correlation (in the far-field) within a single frame from the camera.

Such twin imaging systems can also be used for imaging where one camera directly records an image of the object, and the other camera (or different part of the same camera chip) records only the illumination. Since the spatial distribution of the photons in the two arms is high correlated, the illumination pattern is also almost identical (photon by photon) to that used to illuminate the object. It follows that the subtraction/or division of the two intensity distributions, in principle, can return the transmission of the object with a precision that is better than the shot-noise limit of the detected image alone [23,48]. Figure 7 illustrates the principle of such experiments and shows the denoising of the image of a low absorption object using fluctuation subtraction [49].
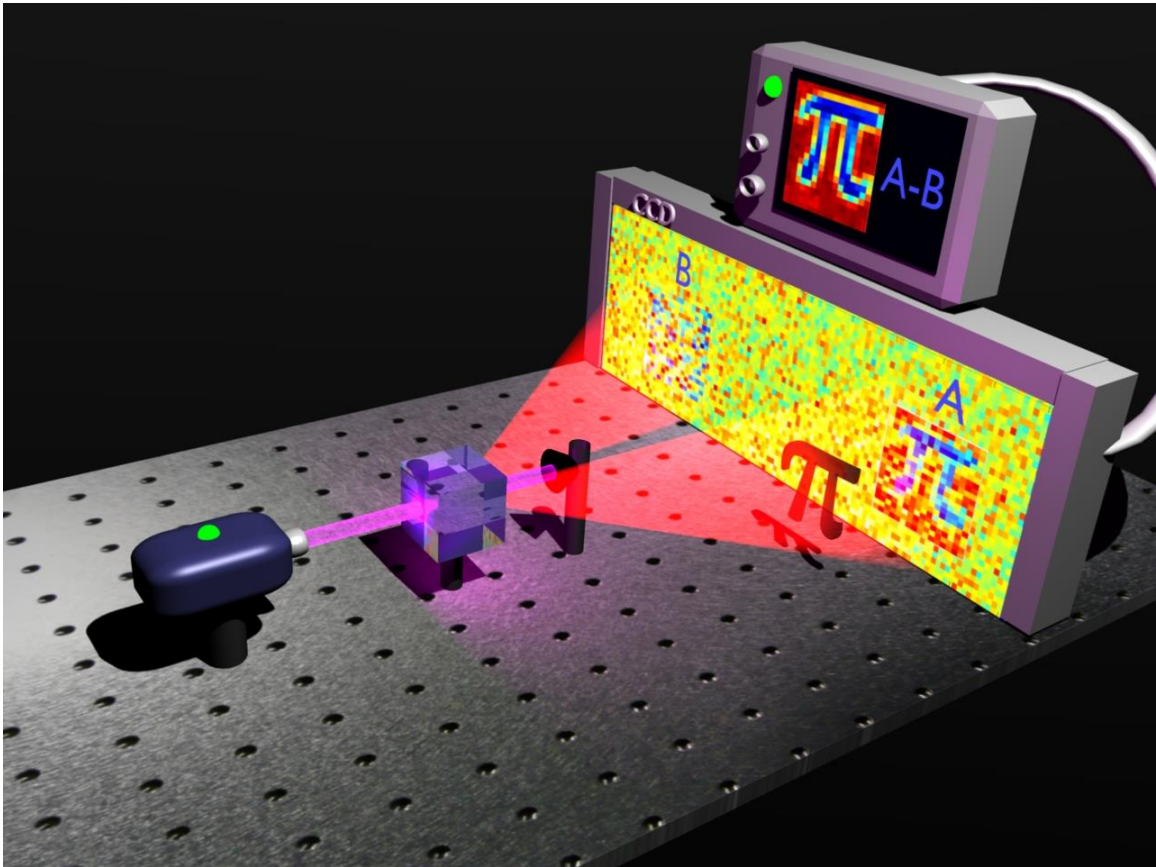
Figure 7: Sub-shot noise imaging of a low absorption sample. Figure reproduced from ref. [49].

This type of sub-shot-noise imaging once again relies upon the spatial correlation that arises as a result of parametric downconversion. More specifically, this imaging technique exploits spatial entanglement, without being itself a proof of it.

Finally, parametric down conversion applications are not limited to intensity imaging, it has been shown that sub shot noise imaging of phase objects can be obtained in the context of microscopy by using NOON states generated by parametric down conversion [50].

11. Ghost imaging based on non-quantum correlations, using thermal light source

The quantum nature of ghost imaging was for a number of years a debated topic, but the issue is now largely resolved. We can practically define quantum ghost imaging as being any ghost imaging scheme enabled by the presence of quantum correlations. On the other hand classical ghost imaging can be defined as being the ensemble of ghost imaging techniques that harness classical correlations. Ghost imaging systems using parametric downconversion are a particular type of quantum ghost imaging and can be based either upon the spatial correlation in the image plane of the downconversion crystal or the spatial anticorrelation in the far-field. If all that is required is a functioning imaging system then either of these is sufficient, without the need of EPR quantum correlations. A specific example of a classical ghost imaging system is one that uses classical correlations from a thermal light source [11,13,51], one will see later that other classes of classical ghost imaging exist – e.g. computational ghost imaging techniques.

In principle, any random light field possess a defined intensity structure. A beam splitter inserted into the beam creates two identical (classical) copies with an experimental 'copy-accuracy', as observed after detecting the intensities of the copied beams, that is limited in principle only by the Poissonian statistics associated with the detected photon-number. In this picture, one copy of the beam is allowed to

propagate to a detector array that measures the exact pattern of the intensity distribution, $P(x, y)_i$, whereas the other copy propagates through exactly the same distance to the object, $O(x, y)$; meaning that the object is illuminated with exactly the same intensity distribution as recorded by the detector array, see Figure 8. It should be noted that the use of an imaging system after the beam splitter in Fig. 8 is unnecessary, as the only requirement is that the camera and the object are positioned in the equivalent plane [13] [15]. The total power of the light transmitted, or backscattered, by the object is measured by a single-pixel detector; this amount constitutes the signal, S_i. Combining the pattern information with the signal information corresponding to many, N, patterns allows one to estimate the image, $I(x, y)$, of the object, as:

$$I(x, y) = \sum_{i=1}^{N} (P(x, y)_i - \langle P(x, y) \rangle) \times (S_i - \langle S \rangle)$$
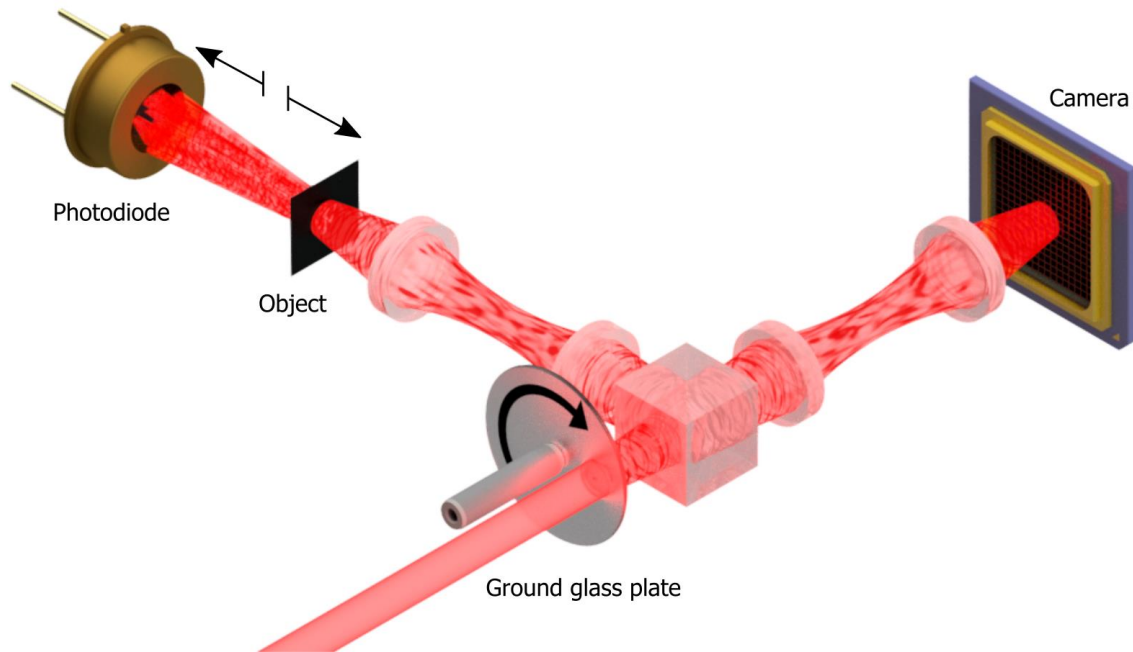

Figure 8: Pseudo-thermal ghost imaging. A coherent light beam passes through a rotating ground glass plate (GGP) thereby generating a series of speckle patterns. The beam is then separated in two using a beam splitter. Finally, the same plane is imaged onto both the object and the camera to ensure that the camera records the pattern projected onto the object. Light transmitted by the object is detected by a photodiode that acts as a bucket detector, its exact position after the object is unimportant. Note that the use of an imaging system after the beam splitter is unnecessary, as the only requirement is that the camera and the object are positioned in the same plane.

In practise, the patterns associated with a true thermal source vary too quickly for a detector array to follow. For this reason, one instead usually adopts a pseudo-thermal source, such as that formed by passing a laser through a rotating ground glass screen. Unlike the photon-pair case, where $P(x, y)_i$ is effectively the position of a single photon and S_i is a binary signal, for this thermal case, $P(x, y)_i$ is a spatially extended function and S_i is an analogue signal. The result of this continuous nature means that the thermal case produces low contrast images, albeit ones that can be dramatically improved by numerical background subtraction [15,52]. The higher flux of a pseudo-thermal source means that once processed, the performance of this classical system can exceed those based upon downconversion [53]. Moreover, it has been shown that the image quality obtained through this technique is resilient to slow acquisition in which many speckle patterns ($\sim$25) are transmitted over the course of a single exposure, thereby allowing the technique to be used with rapidly fluctuating patterns [54]. Some works have claimed that there exists another practical advantage in that, although the presence of turbulence can degrade the quality of the reconstructed images, according to these studies, in some cases, thermal ghost imaging schemes can be designed to be robust against turbulence [55–57], which is claimed to make it a good candidate in remote sensing scenarios [58]. Finally, various reconstruction techniques have been proposed to enhance the signal to noise ratio of the classical ghost imaging methods compared to conventional ghost imaging reconstruction [59,60].

12. Ghost imaging based correlations with structured light fields

Rather than using a ground glass screen, or similar, it is possible to make spatially structured fields using a programmable spatial light modulator (SLM). In this case there is no need for a beam splitter and a detector array to measure the intensity of the light field in the plane of the object, since this pattern can be calculated from knowing the pattern displayed on the SLM. In the original proposal, the SLM was used to create a field of known intensity and phase, such that its intensity structure, $P(x, y)_i$, could be calculated in any subsequent plane. To stress that the correlations

involved are between the light field and the SLM, this technique was called "computational ghost imaging", in an attempt to emphasise its non-quantum nature [43,61].

A more simple configuration that does not require the subsequent computation of the illumination field is to use an intensity modulator, where the plane of the modulator is explicitly imaged to the plane of the object, again giving a known intensity pattern, but this time without need for calculation, see Figure 9. Using spatially structured light to create imaging systems has been known and utilised under various guises for many decades, perhaps the most prevalent being the raster scanning of a laser beam over an object, with the use of a single element detector used to measure the backscattered signal. However, if the source is spatially

Spatial light modulator
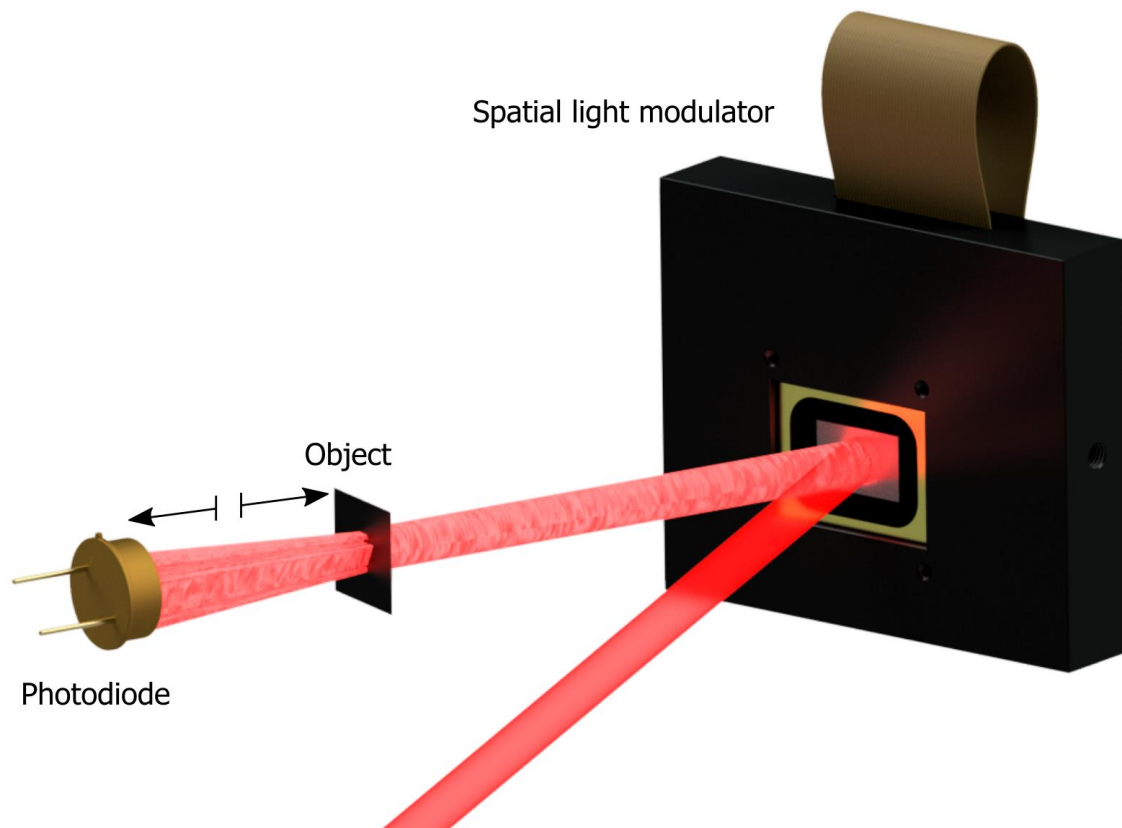
Object

Photodiode

Figure 9 : Computational ghost imaging scheme. An SLM is illuminated by a coherent light source. The spatially modulated light-beam is then sent through or reflected from an object, and a photodiode then detects the overall beam intensity transmitted by or reflected from the object. The Pattern projected onto the object can be deduced from the phase pattern displayed by the SLM. It should be noted that the position of the photodiode is unimportant.

extended then it cannot be focused to form a scanning spot and another approach is needed. Using a spatial light modulator, the spatially extended source can still be structured, allowing the illumination of the object with a known intensity pattern.

Measuring the backscattered signal in response to arbitrary illumination patterns holds further advantages over raster scanning. For a raster-scanned system, the number of measurements required is exactly equal to the number of pixels in the desired image, but if the object is illuminated with a series of extended intensity patterns then the same image can be reconstructed with fewer measurements required. The technique used here is similar in concept to JPEG image compression which works because in the spatial frequency domain typical images are sparse, i.e. they have many frequency components with very low weightings that need not be stored [62,63]. A similar efficiency can also be applied to measurement, allowing an excellent reproduction of an image to be obtained from fewer measurements than there are pixels in the image.

13. Structured illumination imaging systems

Structured illumination is used in various types of imaging systems, for example in the creation of Moiré patterns from which surface shapes can be deduced. However, here we restrict the discussion to the use of structured illumination as a means of single-pixel imaging. Perhaps the most obvious use for structured illumination lies in illumination at wavelengths where traditional imaging based upon focal plane arrays would be expensive, and recently we have adopted this approach for imaging methane gas at ≈1.6μm [64]. Such systems are viable since spatial light modulators work over a wide wavelength range, and cost effective single-pixel detectors are similarly available over a range of different wavelengths.

Another possibility is in the use of multiple detectors, either to extend the wavelength range or to collect light backscattered in different directions. Using multiple detectors located about the object and with known position is akin to photometric imaging. In such a setup, a single structured light source may be used to illuminate an object and the resulting backscattered signal is measured using the

multiple detectors located about the object. This technique enables the gradients of the surface of the object at each pixel to be deduced and subsequently integrated to produce a surface profile. This is achieved by processing a set of simultaneously obtained images of the reflected light generated as a result of illuminating the object with a structured light source, where images that are obtained from a series of detectors at known position relative to the object. Unlike traditional photometric stereo which requires sequential illumination due to there being multiple light
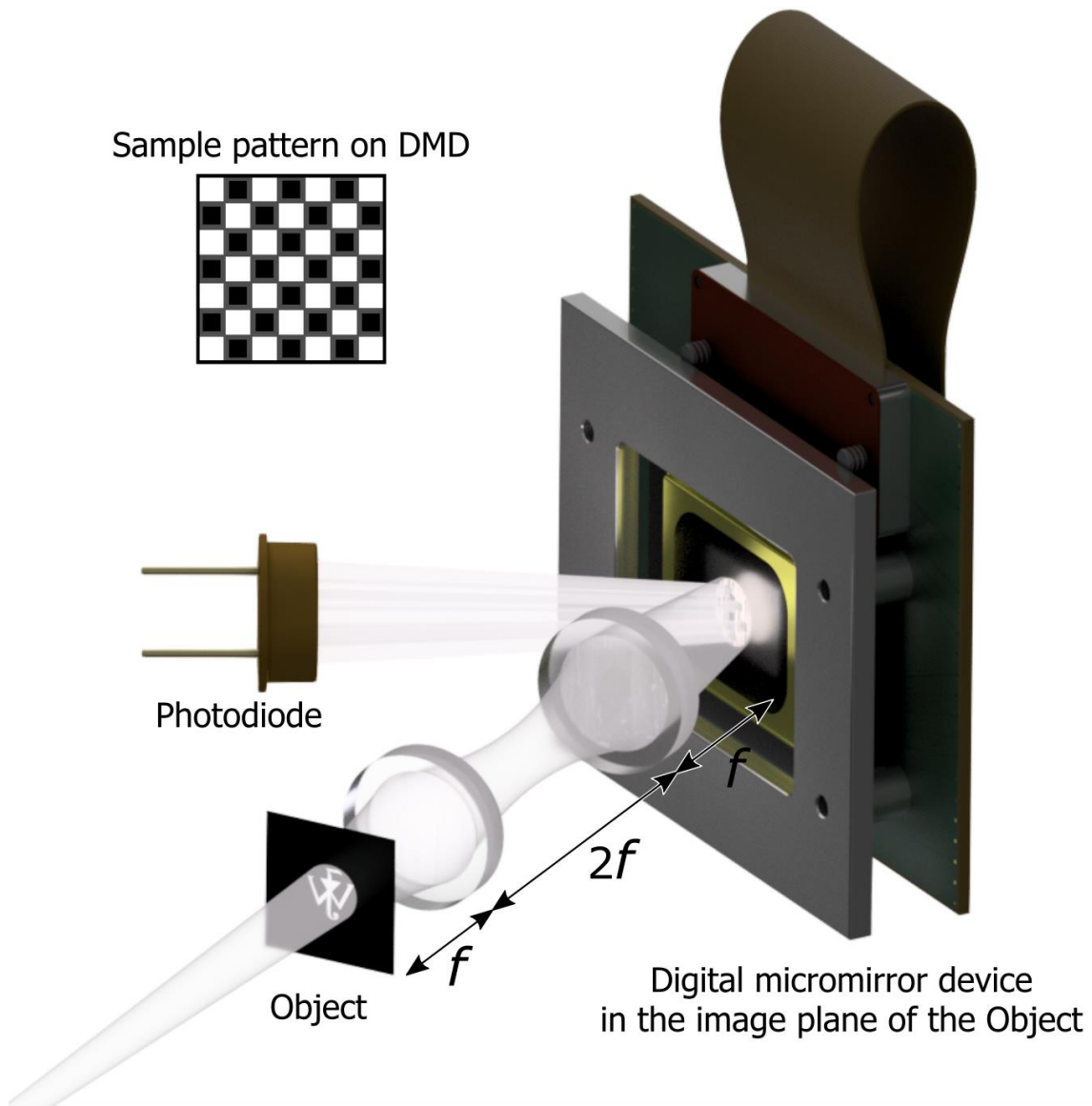

Figure 10: Single-pixel camera's scheme. Coherent or incoherent light is used to illuminate an object. The object plane is imaged onto a DMD that spatially modulates the intensity of the incoming light-beam. A photodiode is used to detect the overall beam intensity reflected by the DMD. It should be noted that the position of the photodiode after the DMD can be arbitrary, as the only requirement is that the full beam is detected.

sources and a single detector, projected illumination requires only sequential patterns and multiple, but simultaneous detections [65].

14. Single-pixel cameras

Although the physics community has developed what we term computational ghost imaging, this whole field is closely related to the broader field of single-pixel cameras as pioneered by Duarte *et al.* [63]. In computational ghost imaging, the data arises from the spatial correlation between the structured illumination and the object. However, the same concept can be employed in a different manner to produce an equivalent result: rather than structuring the illumination, it is possible to structure the detection, simply by replacing the light source with a detector. In this configuration, any light source can be used to illuminate the object that is imaged to the plane of the spatial light modulator or a Digital Micromirror Device (DMD) see Figure 10. The detector now measures the correlation of the backscattered image with the programmed pattern [65]. Figure 11 shows reconstructed images, with data captured using a single pixel camera by Duarte *et al.* [63]. The optimum choice of patterns and algorithms to invert the data formed from both the patterns and the measured signals to obtain an image are largely identical in the computational ghost imaging and single pixel configurations. However, for the single-pixel camera configuration using a DMD there is now less control over the light source, specifically no knowledge of the phase, so calculating the propagating field is problematic. The inability to calculate the general propagation of the field from the plane of the modulator to the plane of the object means that a simpler configuration is to explicitly image the plane of the object to the plane of the modulator and then measure the corresponding intensity correlations with the single-pixel detector.

Single-pixel cameras offer a cost-effective imaging solution for operating at wavelengths were focal plane arrays are expensive or not available. The approach also opens options for hyperspectral imaging, in which multiple single-pixel detectors operating with different wavelength sensitivities can be incorporated into

the same camera system [66–68]. In addition, it has been demonstrated that a single-pixel camera allows the imaging of a scene with a detector that is not placed in direct view of the object [69]. Finally, the high temporal-resolution of single-pixel detectors, compared to focal plane arrays, means that when combined with stroboscopic illumination, it is possible to obtain depth information from the scene, effectively creating an imaging LIDAR [70–72].

(a) (b) (c)
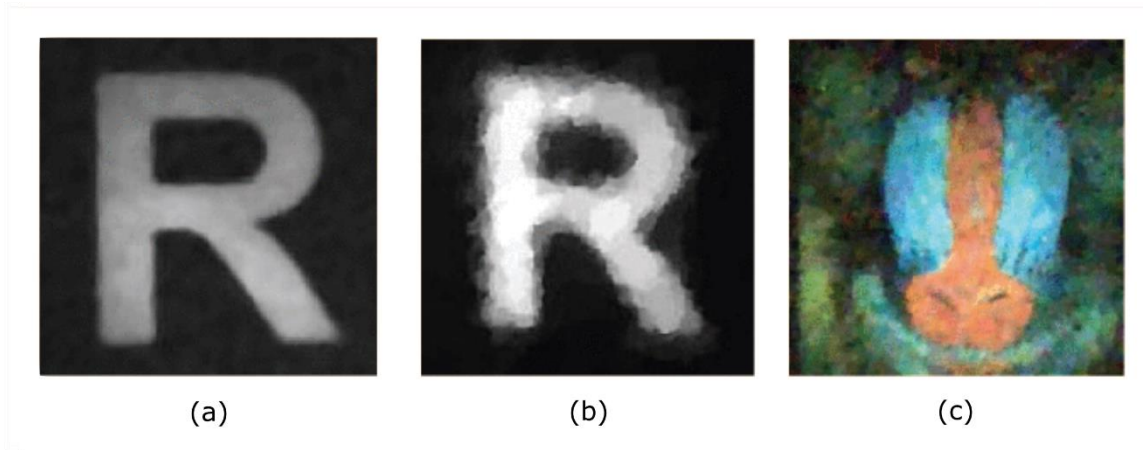
Figure 11: Single-pixel images. (a) Conventional image of a black-and-white letter 'R'. (b) Single-pixel camera reconstructed image from M = 1, 300 random measurements. (c) Colour reconstruction of a printout of the Mandrill standard test image using a single photomultiplier tube sensor and RGB colour filters (M = 6, 500 random measurements). Figure reproduced from ref. [63].

15. Ghost imaging concepts extended to other domains

Since its discovery, the concept of ghost imaging has been extended to domains outside of the capture of spatial proprieties of light and beyond the usual optical domain.

A particularly active research area is that of ghost imaging in the time domain. It was first suggested theoretically [73,74] that a temporal objects could be recorded using a slow integrating 'bucket' detector. It was later demonstrated experimentally [75] using a temporally incoherent source split into two beams so as to record the laser fluctuations on one arm, while the other beam was used to probe the temporal object before being detected by a slow integrating detector unable to

resolve the signal. This demonstration was limited to record temporal signals that are reproducible in time, since as in standard ghost imaging where a large number of patterns must be used in order to reconstruct a ghost image, the temporal signal had in this context to be reproduced many times to allow the statistical reconstruction of the ghost object. The exact space–time transposition of ghost imaging was subsequently reported when it was demonstrated that a non-reproducible signal can be recorded through computational ghost imaging through the use of spatial multiplexing instead of temporal multiplexing [76]. As in the case of standard ghost imaging, it was shown that together with structured light this technique may also exploit both thermal light classical correlations [77] and quantum correlations [78] to retrieve an image of the 'ghost object'.

Finally ghost imaging concepts also apply outside of the usual optical domain. In recently reported experiments, ghost imaging was demonstrated using X-rays [79–81] and for atomic systems through exploiting quantum correlations exhibited by pairs of ultracold helium atoms [82].

16. Conclusions and Outlooks

Since its inception in the 1990's ghost imaging has intrigued researchers, many of whom have been inspired to study this technique, both in terms of the underpinning physics it reveals and for the possible applications it enables. In terms of the underpinning physics, the analysis of images within quantum systems is a study of high-dimensional Hilbert spaces. In terms of applications there seem to be two main avenues of work. Firstly, when using a light source based upon parametric downconversion the temporal correlation allows for a stringent rejection of noise, thereby only requiring very few photons to obtain valuable information about the object/image. Secondly, computational ghost imaging and single-pixel cameras which only require a single-pixel detector to reconstruct the image of an object, allows operation at wavelengths, and on timescales, that would not be possible with focal-plane detector arrays.

A comparatively untapped feature of quantum ghost imaging is that the spatial correlations can be between photons with arbitrary different wavelengths [31,83]. This feature has been used for imaging with short-wave infra-red light while recording the data with a visible wavelength camera. However, there is no fundamental reason why this technique could not be extended to even more inaccessible wavelengths. For example, could this be a route to a low-cost, high-resolution THz camera [84]?

With respect to single-pixel cameras, there seems to be opportunity to relax the "single" to include a small number of detectors, perhaps to create UV-vis-IR images from a single camera. Alternatively, to incorporate additional detection channels to give simultaneous information relating to polarisation, timing/range data or even just to provide complimentary data to a traditional focal plane array.

Future systems seem set to exploit the various elements and algorithms discussed above, from optical-correlations both classical and quantum, compressed sensing and data inversion alongside the ever improving spectral and temporal detector specifications. This future seems both an intellectual adventure and a route to delivering a family of multidimensional cameras operating across a range of wavelengths, timescales and length-scales.

[1]   D. V. Strekalov, A. V. Sergienko, D. N. Klyshko, and Y. H. Shih, Phys. Rev. Lett. 74, 3600 (1995).

[2] T. B. Pittman, Y. H. Shih, D. V. Strekalov, and A. V. Sergienko, Phys. Rev. A. 52, R3429 (1995).

[3] D. N. Klyshko, Sov. Phys. Uspekhi **31**, 74 (1988).

[4] D. Klyshko, Phys. Lett. A **132**, 299 (1988).

[5] S. E. Harris, M. K. Oshman, and R. L. Byer, Phys. Rev. Lett. 18, 732 (1967).

[6] D. A. Kleinman, Phys Rev **174**, 1027 (1968).

[7] D. C. Burnham and D. L. Weinberg, Phys. Rev. Lett. 25, 84 (1970).

[8] T. B. Pittman, D. V. Strekalov, D. N. Klyshko, M. H. Rubin, A. V. Sergienko, and Y. H. Shih, Phys. Rev. A 53, 2804 (1996).

[9] R. S. Bennink, S. J. Bentley, and R. W. Boyd, Phys. Rev. Lett. **89**, 113601 (2002).

[10] A. F. Abouraddy, B. E. A. Saleh, A. V. Sergienko, and M. C. Teich, Phys. Rev. Lett. **87**, 123602 (2001).

[11] A. Gatti, E. Brambilla, M. Bache, and L. A. Lugiato, Phys. Rev. Lett. **93**, 093602 (2004).

[12] Y. J. Cai and S. Y. Zhu, Phys. Rev. E **71**, 056607 (2005).

[13] A. Valencia, G. Scarcelli, M. D'Angelo, and Y. Shih, Phys. Rev. Lett. **94**, 063601 (2005).

[14] F. Ferri, D. Magatti, A. Gatti, M. Bache, E. Brambilla, and L. A. Lugiato, Phys. Rev. Lett. **94**, 183602 (2005).

[15] G. Scarcelli, V. Berardi, and Y. Shih, Phys. Rev. Lett. **96**, 063602 (2006).

[16] B. I. Erkmen and J. H. Shapiro, Phys. Rev. A **77**, 043809 (2008).

[17] B. I. Erkmen and J. H. Shapiro, Adv. Opt. Photonics **2**, 405 (2010).

[18] J. H. Shapiro and R. W. Boyd, Quantum Inf. Process. **11**, 949 (2012).

[19] J. C. Howell, R. S. Bennink, S. J. Bentley, and R. W. Boyd, Phys Rev Lett **92**, 210403 (2004).

[20] M. D'Angelo, Y.-H. Kim, S. P. Kulik, and Y. Shih, Phys. Rev. Lett. **92**, 233601 (2004).

[21] A. Einstein, B. Podolsky, and N. Rosen, Phys. Rev. 47, 777 (1935).

[22] R. S. Aspden, D. S. Tasca, R. W. Boyd, and M. J. Padgett, New J. Phys. **15**, 073032 (2013).

[23] G. Brida, M. Genovese, and I. R. Berchera, Nat. Photonics **4**, 227 (2010).

[24] R. Fickler, M. Krenn, R. Lapkiewicz, S. Ramelow, and A. Zeilinger, Sci. Rep. **3**, 1914 (2013).

[25] M. Sonnleitner, J. Jeffers, and S. M. Barnett, Optica **2**, 950 (2015).

[26] L. Mertens, M. Sonnleitner, J. Leach, M. Agnew, and M. J. Padgett, Sci. Rep., 7, 42164 (2017).

[27] P. A. Morris, R. S. Aspden, J. E. C. Bell, R. W. Boyd, and M. J. Padgett, Nat. Commun. **6**, 5913 (2015).

[28] D. Shin, A. Kirmani, V. K. Goyal, and J. H. Shapiro, IEEE Trans. Comput. Imaging **1**, 112 (2015).

[29] A. Kirmani, D. Venkatraman, D. Shin, A. Colaço, F. N. Wong, J. H. Shapiro, and V. K. Goyal, Science **343**, 58 (2014).

[30] K. W. C. Chan, M. N. O'Sullivan, and R. W. Boyd, Phys. Rev. A **79**, 033808 (2009).

[31] R. S. Aspden, N. R. Gemmell, P. A. Morris, D. S. Tasca, L. Mertens, M. G. Tanner, R. A. Kirkwood, A. Ruggeri, A. Tosi, R. W. Boyd, G. S. Buller, R. H. Hadfield, and M. J. Padgett, Optica 2, 1049 (2015).

[32] G. B. Lemos, V. Borish, G. D. Cole, S. Ramelow, R. Lapkiewicz, and A. Zeilinger, Nature **512**, 409 (2014).

[33] J. H. Shapiro, D. Venkatraman, and F. N. C. Wong, Sci. Rep. **5**, 10329 (2015).

[34] D. A. Kalashnikov, A. V. Paterova, S. P. Kulik, and L. A. Krivitsky, Nat. Photonics **10**, 98 (2016).

[35] R. S. Aspden, D. S. Tasca, A. Forbes, R. W. Boyd, and M. J. Padgett, J. Mod. Opt. **61**, 547 (2014).

[36] E. da S. Fonseca, P. S. Ribeiro, S. Pádua, and C. Monken, Phys. Rev. A **60**, 1530 (1999).

[37] D. Tasca, R. Aspden, P. Morris, G. Anderson, R. Boyd, and M. Padgett, Opt. Express **21**, 30460 (2013).

[38] R. S. Aspden, P. A. Morris, R. He, Q. Chen, and M. J. Padgett, J. Opt. **18**, 055204 (2016).

[39] K. A. Forbes, J. S. Ford, and D. L. Andrews, Phys. Rev. Lett. **118**, 133602 (2017).

[40] P. H. Van Cittert, Phys. Utrecht **1**, 202 (1934).

[41] F. Zernike, Ibid **5**, 785 (1938).

[42] A. Gatti, D. Magatti, and F. Ferri, Phys. Rev. A **78**, 063806 (2008).

[43] J. H. Shapiro, Phys. Rev. A **78**, 061802 (2008).

[44] M. D'Angelo, A. Valencia, M. H. Rubin, and Y. Shih, Phys. Rev. A 72, 013810 (2005).

[45] O. Jedrkiewicz, Y.-K. Jiang, E. Brambilla, A. Gatti, M. Bache, L. Lugiato, and P. Di Trapani, Phys. Rev. Lett. **93**, 243601 (2004).

[46] M. P. Edgar, D. S. Tasca, F. Izdebski, R. E. Warburton, J. Leach, M. Agnew, G. S. Buller, R. W. Boyd, and M. J. Padgett, Nat. Commun. **3**, 984 (2012).

[47] P.-A. Moreau, F. Devaux, and E. Lantz, Phys. Rev. Lett. **113**, 160401 (2014).

[48] E. Brambilla, L. Caspani, O. Jedrkiewicz, L. Lugiato, and A. Gatti, Phys. Rev. A **77**, 053807 (2008).

[49] M. Genovese, G. Brida, A. Meda, and I. R. Berchera, in: Proceedings SPIE 8163, Quantum Communications and Quantum Imaging IX, San Diego, USA, August 2011, pp. 816302.

[50] T. Ono, R. Okamoto, and S. Takeuchi, Nat. Commun., 4, 2426 (2013).

[51] F. Ferri, D. Magatti, A. Gatti, M. Bache, E. Brambilla, and L. A. Lugiato, Phys. Rev. Lett. **94**, 183602 (2005).

[52] R. S. Bennink, S. J. Bentley, R. W. Boyd, and J. C. Howell, Phys. Rev. Lett. **92**, 033601 (2004).

[53] A. Gatti, E. Brambilla, M. Bache, and L. A. Lugiato, Phys. Rev. A **70**, 013802 (2004).

[54] P. Zerom, Z. Shi, M. N. O'Sullivan, K. W. C. Chan, M. Krogstad, J. H. Shapiro, and R. W. Boyd, Phys. Rev. A **86**, 063817 (2012).

[55] J. Cheng, Opt. Express **17**, 7916 (2009).

[56] R. E. Meyers, K. S. Deacon, and Y. Shih, Appl. Phys. Lett. **98**, 111115 (2011).

[57] R. E. Meyers, K. S. Deacon, and Y. Shih, Appl. Phys. Lett. **100**, 131114 (2012).

[58] B. I. Erkmen, J. Opt. Soc. Am. A-Opt. Image Sci. Vis. 29, 782 (2012).

[59] F. Ferri, D. Magatti, L. A. Lugiato, and A. Gatti, Phys. Rev. Lett. **104**, 253603 (2010).

[60] B. Sun, S. S. Welsh, M. P. Edgar, J. H. Shapiro, and M. J. Padgett, Opt. Express **20**, 16892 (2012).

[61] Y. Bromberg, O. Katz, and Y. Silberberg, Phys. Rev. A **79**, 053840 (2009).

[62] O. Katz, Y. Bromberg, and Y. Silberberg, Appl. Phys. Lett. **95**, 131110 (2009).

[63] M. F. Duarte, M. A. Davenport, D. Takbar, J. N. Laska, T. Sun, K. F. Kelly, and R. G. Baraniuk, IEEE Signal Process. Mag. **25**, 83 (2008).

[64] G. M. Gibson, B. Sun, M. P. Edgar, D. B. Phillips, N. Hempler, G. T. Maker, G. P. A. Malcolm, and M. J. Padgett, Opt Express **25**, 2998 (2017).

[65] B. Sun, M. P. Edgar, R. Bowman, L. E. Vittert, S. Welsh, A. Bowman, and M. J. Padgett, Science **340**, 844 (2013).

[66] S. S. Welsh, M. P. Edgar, R. Bowman, P. Jonathan, B. Sun, and M. J. Padgett, Opt. Express **21**, 23068 (2013).

[67] D.-J. Zhang, H.-G. Li, Q.-L. Zhao, S. Wang, H.-B. Wang, J. Xiong, and K. Wang, Phys. Rev. A **92**, 013823 (2015).

[68] M. P. Edgar, G. M. Gibson, R. W. Bowman, B. Sun, N. Radwell, K. J. Mitchell, S. S. Welsh, and M. J. Padgett, Sci. Rep. **5**, 10669 (2015).

[69] Z. Zhang, X. Ma, and J. Zhong, Nat. Commun. **6**, 6225 (2015).

[70] G. A. Howland, D. J. Lum, M. R. Ware, and J. C. Howell, Opt. Express **21**, 23822 (2013).

[71] N. D. Hardy and J. H. Shapiro, Phys. Rev. A **87**, 023820 (2013).

[72] M.-J. Sun, M. P. Edgar, G. M. Gibson, B. Sun, N. Radwell, R. Lamb, and M. J. Padgett, Nat. Commun., 7, 12010 (2016).

[73] T. Shirai, T. Setälä, and A. T. Friberg, J. Opt. Soc. Am. B 27, 2549 (2010).

[74] T. Setälä, T. Shirai, and A. T. Friberg, Phys. Rev. A **82**, 043813 (2010).

[75] P. Ryczkowski, M. Barbier, A. T. Friberg, J. M. Dudley, and G. Genty, Nat. Photonics **10**, 167 (2016).

[76] F. Devaux, P.-A. Moreau, S. Denis, and E. Lantz, Optica **3**, 698 (2016).

[77] F. Devaux, K. P. Huy, S. Denis, E. Lantz, and P.-A. Moreau, J. Opt. **19**, 024001 (2016).

[78] S. Denis, P.-A. Moreau, F. Devaux, and E. Lantz, J. Opt. **19**, 034002 (2017).

[79] J. Cheng and S. Han, Phys. Rev. Lett. **92**, 093903 (2004).

[80] D. Pelliccia, A. Rack, M. Scheel, V. Cantelli, and D. M. Paganin, Phys. Rev. Lett. **117**, 113902 (2016).

[81] H. Yu, R. Lu, S. Han, H. Xie, G. Du, T. Xiao, and D. Zhu, Phys. Rev. Lett. **117**, 113901 (2016).

[82] R. I. Khakimov, B. Henson, D. Shin, S. Hodgman, R. Dall, K. Baldwin, and A. Truscott, Nature **540**, 100 (2016).

[83] S. Karmakar and Y. Shih, Phys. Rev. A **81**, 033845 (2010).

[84] V. V. Kornienko, S. A. Savinov, Y. A. Mityagin, and G. K. Kitaeva, Opt. Lett. **41**, 4075 (2016).